AGU PUBLICATIONS

JGR

Journal of Geophysical Research: Space Physics

TECHNICAL REPORTS: METHODS

10.1002/2014JA020899

Modeling geomagnetic cutoffs for space weather applications

B. T. Kress[1,2], M. K. Hudson[3], R. S. Selesnick[4], C. J. Mertens[5], and M. Engel[3]

[1]Cooperative Institute for Research in Environmental Sciences, University of Colorado Boulder, Boulder, Colorado, USA, [2]National Geophysical Data Center, National Oceanic and Atmospheric Administration, Boulder, Colorado, USA, [3]Department of Physics and Astronomy, Dartmouth College, Hanover, New Hampshire, USA, [4]Space Vehicles Directorate, Air Force Research Laboratory, Kirtland AFB, Albuquerque, New Mexico, USA, [5]NASA Langley Research Center, Hampton, Virginia, USA

Key Points:
- A method for computing effective cutoff rigidities is described
- Poor convergence of modeled upper and lower cutoffs is shown
- Error of using $1/L^2$ to scale modeled cutoffs is presented

Correspondence to:
B. T. Kress,
bkress@northstar.dartmouth.edu

Citation:
Kress, B. T., M. K. Hudson, R. S. Selesnick, C. J. Mertens, and M. Engel (2015), Modeling geomagnetic cutoffs for space weather applications, *J. Geophys. Res. Space Physics*, *120*, 5694–5702, doi:10.1002/2014JA020899.

Received 19 MAR 2015
Accepted 1 JUN 2015
Accepted article online 4 JUN 2015
Published online 14 JUL 2015

Abstract Access of solar and galactic cosmic rays to the Earth's magnetosphere is quantified in terms of geomagnetic cutoff rigidity. Numerically computed grids of cutoff rigidities are used to model cosmic ray flux in Earth's atmosphere and in low Earth orbit. In recent years, the development of more accurate dynamic geomagnetic field models and an increase in computer power have made a real-time data-driven geomagnetic cutoff computation extending over the inner magnetosphere possible. For computational efficiency, numerically computed cutoffs may be scaled to different altitudes and directions of arrival using the known analytic variation of cutoff in a pure dipole magnetic field. This paper is a presentation of numerical techniques developed to compute effective cutoff rigidities for space weather applications. Numerical tests to determine the error associated with scaling vertical cutoff rigidities with altitude in a realistic geomagnetic field model are included. The tests were performed to guide the development of spatial grids for modeling cosmic ray access to the inner magnetosphere and to gain a better understanding of the accuracy of numerically modeled cutoffs.

1. Introduction

It was recognized in the 1960s that solar and galactic cosmic rays penetrate further into the magnetosphere than is predicted using a pure dipole model of the Earth's magnetic field [*Lanzerotti*, 1968; *Fillius*, 1968; *Paulikas and Blake*, 1969]. The effect of addition of higher order moments, in a spherical harmonic expansion of the Earth's magnetic field, is to reduce shielding of energetic ions by the main dipole field [e.g., *Kress et al.*, 2013]. In general, the addition of magnetospheric current systems further reduces geomagnetic shielding of energetic ions incident from interplanetary space. Using energetic particle measurements from the Solar Anomalous and Magnetospheric Particle Explorer (SAMPEX), *Leske et al.* [2001] showed that the suppression of geomagnetic shielding of solar cosmic rays (also called solar energetic particles) is correlated with the depression and recovery of the disturbance storm time (*Dst*) index, thus is primarily attributed to a reduction in field strength in the inner magnetosphere due to ring current buildup.

While the bulk of the solar wind is deflected around the magnetosphere, cosmic rays with energies in the tens of MeV and greater have direct access to the inner magnetosphere. During quiet geomagnetic periods, solar protons with energies from 10 to 500 MeV typically penetrate to $L \sim 4$. Galactic cosmic rays with GeV energies and greater can penetrate to lower L shells, and protons with energies $\gtrsim$ 15 GeV have access to the Earth's upper atmosphere at equatorial latitudes. The amount a particle is deflected by a magnetic field is determined by its rigidity (momentum per unit charge). *Störmer* [1955, and references therein] showed that in a magnetic dipole there is a *cutoff* rigidity (henceforth simply "cutoff"), corresponding to each location and direction of arrival. The cutoff is the threshold rigidity below which the particle flux is zero due to magnetic shielding.

Energetic particle cutoffs can be determined numerically in a geomagnetic field model. Numerical results obtained by computing Lorentz trajectories in geomagnetic field models that included magnetospheric boundary currents, tail currents, and the ring current are found to significantly improve agreement between observed and theoretically predicted cosmic ray cutoffs [*Taylor*, 1967; *Smart et al.*, 1969]. Improvement over cutoffs analytically determined in a pure dipole model of the geomagnetic field were also obtained using approximate analytic methods developed by *Sauer* [1963], which include the effect of nondipolar terms in a spherical harmonic expansion of the Earth's magnetic field. In spite of improvements in geomagnetic field

models since the 1960s, high-latitude cutoffs computed in state of the art magnetic field models are in general too high [*Kahler and Ling*, 2002; *Kress et al.*, 2010, 2013].

Grids of geomagnetic cutoff rigidities computed in a geomagnetic field model are used to model the flux of solar energetic particles and galactic cosmic rays in the Earth's inner magnetosphere and upper atmosphere for space weather applications [*Smart and Shea*, 2003; *Smart et al.*, 2006]. Computing global maps of cutoff rigidities is computationally intensive requiring millions of particle trajectories. In recent years, advancements in computing power and the development of more accurate dynamic geomagnetic field models have made real-time data-driven geomagnetic cutoff rigidity calculations possible. A real-time cutoff model, developed by the Center for Integrated Space Weather Modeling (CISM) at Dartmouth College is being used in conjunction with the High Energy and Charge Transport code for the development of the Nowcast of Atmospheric Ionizing Radiation for Aviation Safety (NAIRAS) model, supported by the NASA Applied Sciences Program [*Mertens et al.*, 2010; *Kress et al.*, 2010]. The NAIRAS model is a prototype operational model that provides global, real-time, data-driven predictions of atmospheric ionizing radiation exposure for archiving and assessing radiation levels at commercial airline altitudes. The CISM-Dartmouth cutoff rigidity model provides a dynamic outer boundary condition for the NAIRAS model. Cutoff rigidities are computed on a grid at 100 km to model solar and galactic cosmic ray access to the Earth's upper atmosphere.

Single event upsets produced by solar and galactic cosmic rays are thought to be a primary source of operational failures in microelectronics on board Earth orbiting spacecraft [*Tylka et al.*, 2005]. Growing dependence on spacecraft in low Earth orbit (LEO), middle Earth orbit, and at geosynchronous have increased the need for extension of cutoff models throughout the inner magnetosphere. Cutoff rigidity in the inner magnetosphere varies with location and direction of arrival. Cutoff rigidities numerically modeled on a grid can be interpolated to locations between grid nodes using the known analytic variation of cutoff in a pure dipole magnetic field. Since the geomagnetic field deviates from a pure dipole, there is error associated with the interpolation. To minimize computational effort, it is necessary to determine what grid resolution is needed to scale the cutoffs to within a given error tolerance. This paper contains the results of a series of numerical tests performed to determine the error due to scaling cutoffs with altitude. Numerical tests of scaling to different directions of arrival will be included in a separate paper. Cutoffs are computed in International Geomagnetic Reference Field (IGRF) and *Tsyganenko and Sitnov* [2005] (TS05) geomagnetic field models. The scaling accuracy tests are not an exhaustive error analysis of all possible locations, directions, and magnetospheric configurations. The tests are aimed at providing information needed to guide development of a grid and to gain a better understanding of the accuracy of the numerically computed cutoffs. New techniques for computing an effective cutoff rigidity R_C, which include the effect of the Earth's shadow (penumbra), are also presented. A good understanding of the accuracy of the cutoff determination is necessary to compare scaling to direct computation. The rapid convergence of R_C with increasing sampling density is demonstrated. This work builds on previous work by *Smart and Shea* [2009, and references therein].

2. Background

In a pure dipole field the cutoff rigidity can be expressed analytically:

$$R_S = C_{St} \frac{1}{L^2} \frac{1}{\left(1 + \sqrt{(1 + \cos\alpha \cos^3\lambda)}\right)^2}, \tag{1}$$

where $L = r/\cos^2\lambda$ is the dipole L shell, λ is the magnetic latitude, α is the angle between the particle arrival direction and magnetic west, and $C_{St} = 60$ is a constant containing the dipole moment (8.06×10^{25} Gauss cm^3) and the conversion factors necessary to express R_C in units of GV [*Störmer*, 1955]. In equation (1), following *Cooke et al.* [1991], the S subscript is used to distinguish the *Störmer* [1955] cutoff in a pure dipole from cutoff rigidity in an arbitrary geomagnetic field model. Although Störmer's analytic result is derived in a pure dipole magnetic field, *Ray* [1963] showed the existence of nonaxissymmetric cutoffs in fields expressible by Euler potentials. Also, well-defined geomagnetic cutoffs are found in observations and numerical results [e.g., *Leske et al.*, 2001; *Kress et al.*, 2010]. Cutoff rigidities in the Earth's magnetosphere are in general a function of location, direction of arrival, and geomagnetic activity.

Assuming an isotropic particle flux in interplanetary space, Liouville's theorem requires that at rigidities above the cutoff rigidity, the directional flux of particles in the magnetosphere is equivalent to that outside the influence of the geomagnetic field [*Lemaitre and Vallarta*, 1933; *Swann*, 1933]. The differential directional flux at a

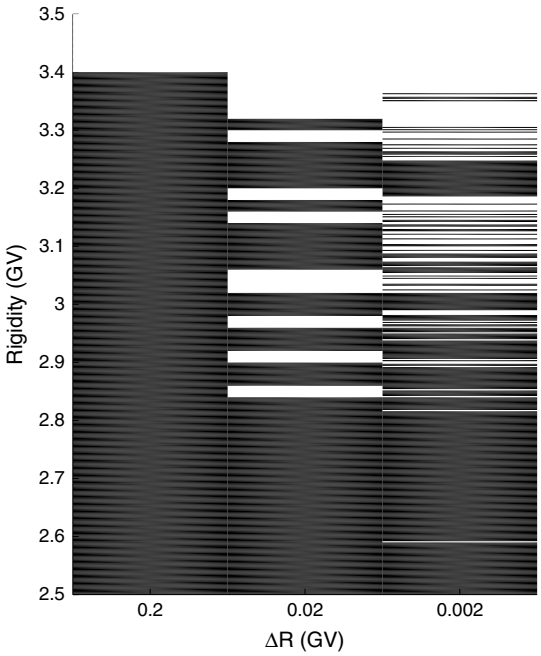

Figure 1. Structure of the penumbral region revealed by sampling the penumbral region with greater resolution, using rigidity step sizes $\Delta R = 0.2$, 0.02, and 0.002 GV. Black indicates forbidden trajectories, and white indicates allowed trajectories.

location in the magnetosphere is modeled by taking the portion of the interplanetary spectrum with rigidities exceeding the cutoff rigidity.

A model of solar and galactic cosmic rays in the magnetosphere based on numerically computed cutoffs is complicated by addition of the solid body of the Earth. In the Earth's upper atmosphere and in low Earth orbit $\sim 2\pi$ sr are blocked by the Earth reducing the flux by approximately one half. In space, since the cutoff rigidity is lowest for particles arriving from the west, the maximum cosmic ray flux is from the west. In the Earth's upper atmosphere the direction of arrival of the maximum cosmic ray flux approaches the zenith since cosmic rays arriving from the vertical direction are least attenuated by collisions with atmospheric constituents. In early studies involving atmospheric measurements this led to the use of the vertical cutoff rigidity R_{CV} [*Smart and Shea*, 1994].

The vertical cutoff rigidity in the pure dipole approximation is obtained by setting $\alpha = \pi/2$ in equation (1):

$$R_{CV} = \frac{C_{St}}{4L^2}, \tag{2}$$

There is very little variation in cutoff rigidity with direction of arrival for high-latitude cutoffs [e.g., see *Kress et al.*, 2013, Figure 1]. This justifies use of vertical cutoff rigidities for modeling omnidirectional cosmic ray flux in LEO. Vertical cutoff rigidities are not appropriate for modeling cosmic ray flux incident from all arrival directions in geosynchronous or other equatorial orbits. An approximation for the cutoff rigidity is obtained by replacing L in equation (2) with the *McIlwain* [1961] L_M parameter: $R_M = C_{St}/(4L_M^2)$ [*Smart et al.*, 2006]. Use of L_M in equation (2) includes the effect of the azimuthal asymmetry of the geomagnetic field.

Since particle trajectories are bent due to the influence of the magnetic field, some trajectories arriving from directions above the Earth's horizon are also blocked by the Earth, including some trajectories arriving from the zenith direction. The result is a shadow or penumbral region containing bands of forbidden and allowed trajectories at rigidities above the magnetic cutoff rigidity. In order to characterize the penumbral region, one may define a *lower vertical cutoff rigidity* R_L below which all particle trajectories are shielded, either by the solid body of the Earth or due to magnetic shielding, and an *upper vertical cutoff rigidity* R_U above which all trajectories are allowed. To account for the penumbral region, an effective cutoff rigidity R_C between R_L and R_U may be used for space weather applications [*Smart et al.*, 2006].

3. Numerically Modeled Geomagnetic Cutoffs

The standard technique for numerically modeling geomagnetic cutoffs is to compute time-reversed Lorentz trajectories in a geomagnetic field model [*Smart et al.*, 2000]. Particle trajectories are initiated at a location in the model fields to test cosmic ray access to that location. If a particle escapes the magnetosphere, then a viable inward trajectory has been found, indicating that the particle's rigidity is above the cutoff rigidity. By testing trajectories over a range of rigidities at a given location and direction of arrival, a numerical search algorithm can be used to locate the threshold rigidity below which there are no allowed trajectories, designated the cutoff rigidity.

A straightforward approach for determining R_L is to successively test incrementally higher rigidities until an escaped trajectory indicates the lower cutoff rigidity has been exceeded. A numerical search for the cutoff rigidity is complicated by the penumbra. The penumbral region between R_L and R_U is a mixture of allowed and forbidden trajectories. A rigidity step size of 0.01 GV, for example, does not assure that R_L is determined to

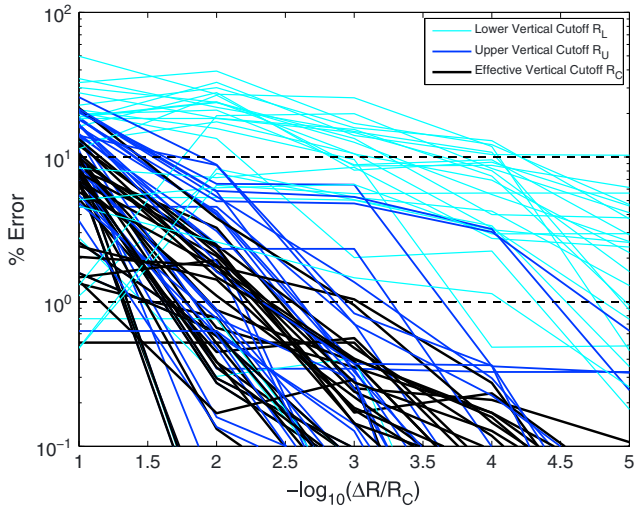

Figure 2. Convergence of lower (R_L), upper (R_U), and effective (R_C) cutoff rigidities with increased sampling resolution. The dashed lines at 1% error and 10% error are included for reference. Error associated with R_L is ~10% when the penumbra is sampled at uniformly spaced rigidity steps with $\Delta R \sim R/10^5$.

within 0.01 GV accuracy. A band of rigidities corresponding to allowed trajectories may occupy a narrow range of rigidities missed by 0.01 GV steps resulting in a significant error in R_L. Similar conclusions about numerical cutoff determinations have been noted previously [*Pchelkin and Vashenyuk*, 2001; *Pchelkin et al.*, 2007].

Figure 1 illustrates the increasingly fine structure revealed by sampling the penumbral region with greater resolution. Figure 1 was produced by computing time-reversed Lorentz trajectories in the IGRF field model, initiated in the zenith direction at 100 km altitude, 40° latitude, 40° longitude. The trajectories were tested at uniformly spaced rigidity intervals $\Delta R = 0.2$, 0.02, and 0.002 GV. Black indicates forbidden trajectories, and white indicates allowed trajectories. In each case the white and black bands are centered on the sampled rigidity, e.g., in the case with $\Delta R = 0.2$ GV, the sampled rigidities include 3.1, 3.3, 3.5..., and we obtain $R_L = R_U = 3.4$ GV. In the case with $\Delta R = 0.002$ GV, the values determined for R_L and R_U are 2.590 GV and 3.362 GV, respectively. The white band at $R_L = 2.590$ GV corresponds to a single allowed trajectory. A decrease in rigidity step size from, e.g., 0.001% of R_C to 0.0001% of R_C can reduce the numerically determined value for R_L by as much as 10%. This slow convergence makes a search for the lower vertical cutoff rigidity computationally prohibitive. However, the location of the R_L is of little practical interest in this case, since the lower portion of the penumbra contains mostly forbidden trajectories and does not significantly contribute to total flux.

An effective cutoff rigidity for space weather applications can be defined

$$R_C = R_L + (R_U - R_L) \times N_{\text{forbidden}}/N_{\text{total}}, \tag{3}$$

where $N_{\text{forbidden}}$ and N_{total} are the number of forbidden trajectories and total sampled trajectories, in the region of rigidity space between R_L and R_U. R_L and R_U are rigidities corresponding to the lowest rigidity allowed trajectory and highest rigidity forbidden trajectory in the sampled portion of rigidity space [*Shea et al.*, 1965]. Below, we show that R_C is not sensitive to the upper and lower boundaries of the sampled region, providing the lower boundary is in a region of mostly forbidden trajectories and the upper boundary is in a region of mostly allowed trajectories.

The convergence of R_L, R_U, and R_C with decreasing rigidity step size is shown in Figure 2. R_L, R_U, and R_C were determined repeatedly using step sizes $\Delta R = R \times 10^{-n}$ with $n = 1 - 6$, here using uniformly spaced steps in rigidity space. The lower, upper, and effective vertical cutoff rigidities are computed in the IGRF-10 field model, using epoch 2000 coefficients, at 100 km, at geographic latitudes from −85° to 85° in steps of 5°, and at 0° longitude. The error is calculated using cutoffs determined with $\Delta R = R \times 10^{-6}$ as accepted/correct values. The dashed lines at 1% error and at 10% error are included for reference. R_C is determined to within ~ 1% accuracy by sampling rigidity space with density $1000/R_C$.

Effective cutoff rigidities R_C presented in the remainder of this paper are determined using an iterative Monte Carlo method, where successively larger regions of rigidity space are randomly sampled with density $1000/R_M$ until the change in R_C is less than 1%. R_M is used as an initial estimate of the cutoff, to locate the region of rigidity space where the sampling begins.

Lorentz trajectories are computed using a fourth-order Runge-Kutta integrator using single (≈ 8 digit) precision floating point variables. The time step is continuously adapted to be 1/100 of the particle gyroperiod. Fast integration is achieved by linearly interpolating magnetic fields from a Cartesian grid to the particle

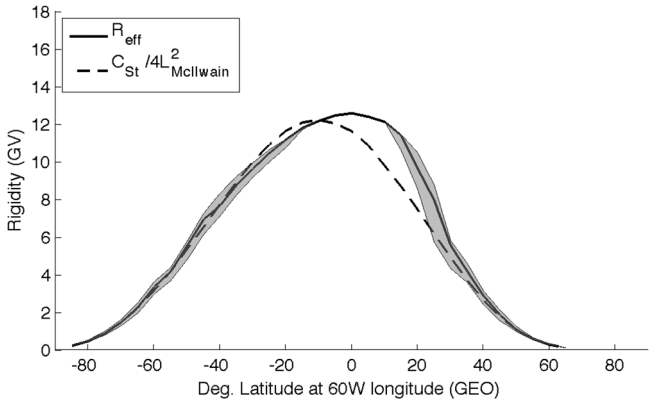

Figure 3. Cutoff rigidity versus latitude determined in the IGRF field model at 60°W longitude (GEO), where there is significant difference between R_C and R_M. The gray-shaded area is the penumbral region bounded by lower and upper cutoff rigidities.

position. Prior to computing particle trajectories, the magnetic field is loaded onto a regular Cartesian grid in computer RAM. The grid spacing is $\Delta x = \Delta y = \Delta z = 0.1$ Earth radii (R_E). A pure analytic dipole field is subtracted from the gridded fields then added back in following each linear interpolation to the particle position so that the linear interpolation error is restricted to the perturbation field.

4. Scaling Magnetospheric Cutoffs Using Störmer Analytic Relation

Replacement of dipole L in equation (2) with the *McIlwain* [1961] L_M parameter provides an approximation for geomagnetic cutoffs [*Shea et al.*, 1985]. In general, R_M is less than R_C due to the penumbra, with the greatest error in the midlatitudes. The percent error approaches 30% in the north Atlantic due to combined effect of the Earth's offset dipole and the longitudinal phase shift of cutoff rigidity contours with respect to contours of magnetic field strength. Figure 3 shows a comparison between R_C and R_M versus latitude at 60°W longitude computed in the IGRF field model. The relative error is approximately 30% near +20° latitude. The gray-shaded area surrounding R_C is the penumbral region, bounded by R_L and R_U.

The $1/L^2$ dependence of vertical cutoff rigidity in a pure dipole suggests scaling cutoff with altitude at fixed latitude, longitude, and look direction using

$$R_{\text{scaled}} = \left(L_{M\,1}^2 / L_{M\,2}^2\right) R_{C\,1}, \tag{4}$$

where $L_{M\,1}$ is the L-McIlwain parameter at the altitude where $R_{C\,1}$ is calculated directly and $L_{M\,2}$ is L-McIlwain at the altitude scaled to. Use of L-McIlwain gives better results than, e.g., dipole L in the geomagnetic coordinate system.

As an example, Figure 4 shows the percent relative error incurred using equation (4) to scale numerically determined cutoff rigidities from 100 km to 600 km altitude. Figure 4 (left) shows the error computed in the IGRF field model, and Figure 4 (right) shows the error computed in the TS05 model fields during a quiet geomagnetic period (TS05Q). The percent relative error is calculated $100\times(R_{\text{scaled}} - R_C)/R_C$. The root-mean-square error (RMSE) and maximum absolute value of errors (MAXE) in this case are 2.43% and 14.0%, respectively. The white areas in Figure 4 are regions where the cutoff rigidity is near or below 0.1 GV (corresponding to a

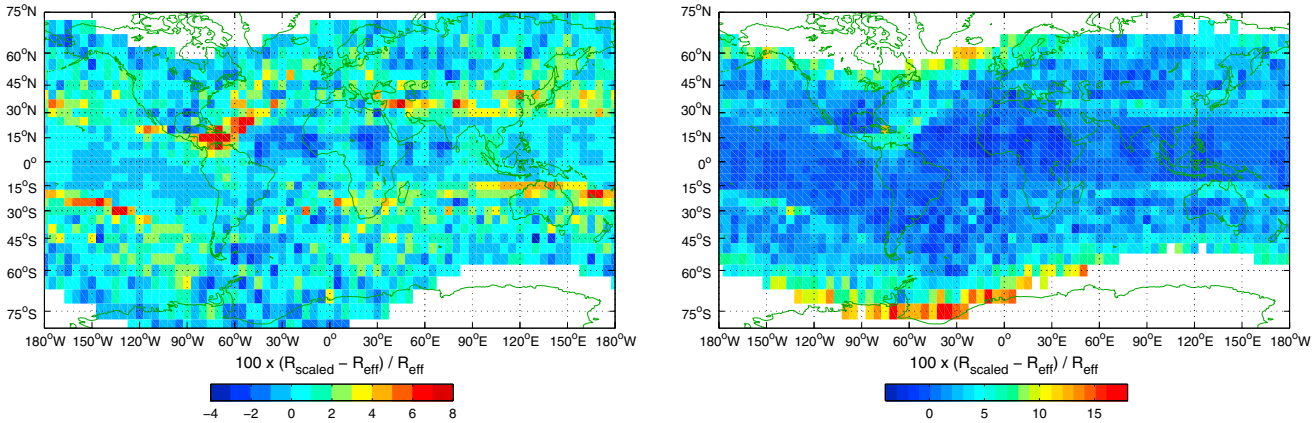

Figure 4. Relative error of using $1/L_M^2$ dependence to scale vertical cutoff rigidities from 100 to 600 km altitude in the (left) IGRF and (right) TS05Q field models.

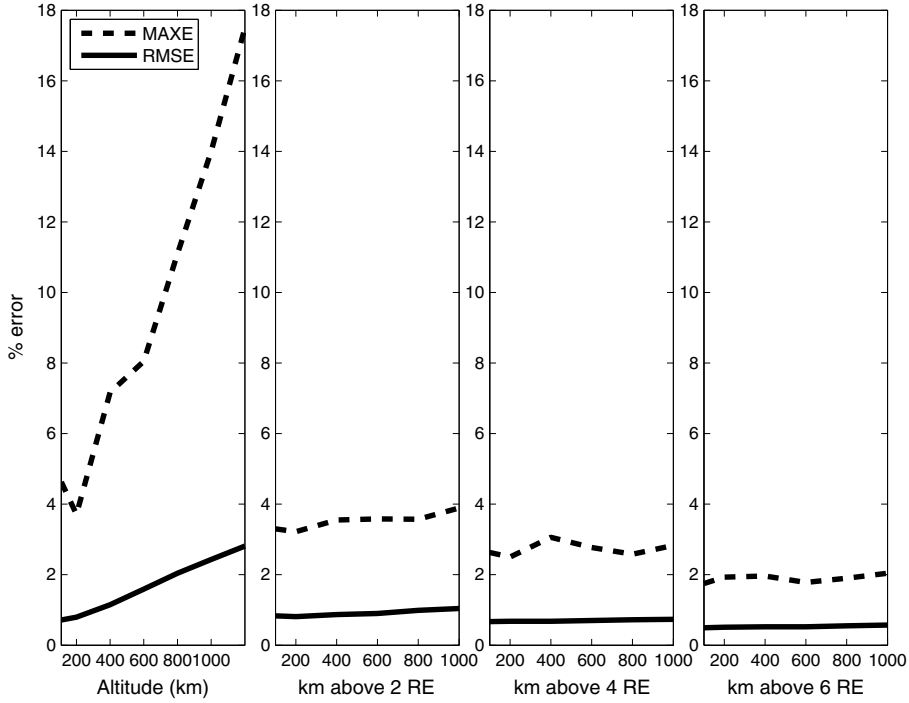

Figure 5. The $1/L_M^2$ scaling error versus altitude in IGRF field model. The relative error due to scaling vertical cutoff rigidities at 100 km, 2 R_E (Earth radii), 4 R_E, and 6 R_E to locations 100–1000 km above these altitudes is shown.

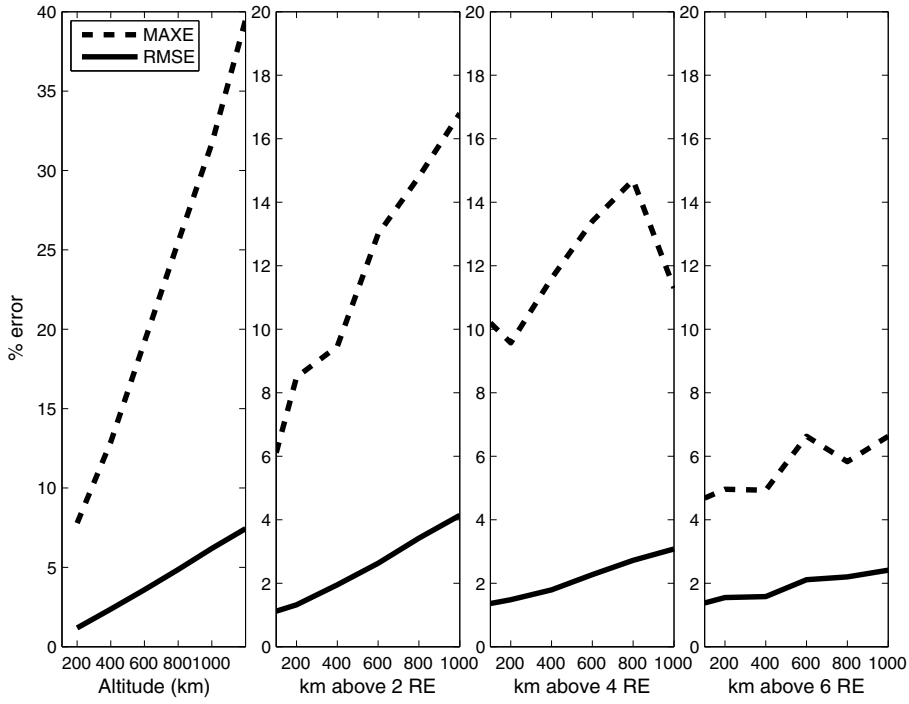

Figure 6. The $1/L_M^2$ scaling error versus altitude in TS05Q field model. The relative error due to scaling vertical cutoff rigidities at 100 km, 2 R_E, 4 R_E and 6 R_E to locations 100-1000 km above these altitudes is shown.

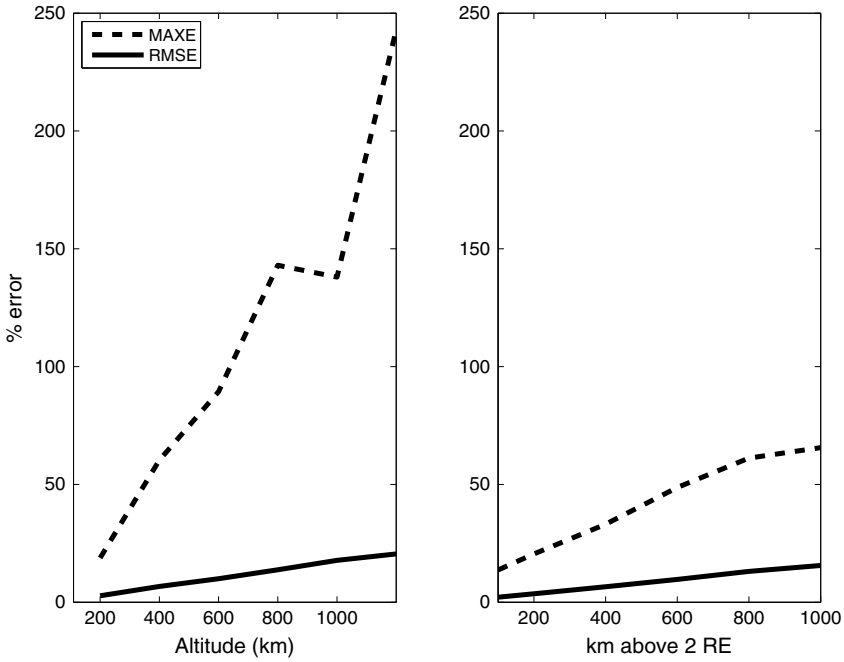

Figure 7. The $1/L_M^2$ Scaling error versus altitude in TS05S field model. The relative error due to scaling vertical cutoff rigidities at 100 km and 2 R_E to locations 100-1000 km above these altitudes is shown. In the TS05S field model, geomagnetic cutoffs drop to zero at and above $\sim$ 4 R_E.

5 MeV proton). The RMSE is calculated using differences between R_{scaled} and R_C at all locations on the latitude-longitude grid where the cutoff is > 0.1 GV, at both 100 km and 1000 km. At higher altitudes the portion of the latitude-longitude grid where cutoffs are above 0.1 GV is restricted to an increasingly smaller range of latitudes.

Scaling error tests using equation (4) are summarized in Figures 5–7. Numerical errors were computed for altitudes near 100 km, 2, 4, and 6 R_E. Cutoff rigidities computed using Lorentz trajectories are compared with scaled cutoff rigidities at distances of 100–1000 km above these altitudes. The cutoffs are computed on a 5°×5° latitude-longitude grid including latitudes −85° to 85° and longitudes 0° to 355° in geographic coordinates. Figures 5–7 correspond to three cases: the IGRF-10 field model using epoch values from year 2000 with degree and order 13, TS05 during a quiet geomagnetic period (TS05Q), and TS05 during an extreme geomagnetic storm (TS05S). The TS05 quiet and storm cases use input parameters corresponding to dates and times the day before and during the 29–31 October 2003 geomagnetic storm. These dates are chosen somewhat arbitrarily but are representative of a typical quiet geomagnetic period and an extreme case, where the *Dst* index drops to near −300 nT. The error is in general smallest in the IGRF field model, as expected since it is more dipolar. The scaling error is greater in the more realistic TS05Q field, and greatest in the TS05S field. Also, the scaling is in general better at higher altitudes.

5. Summary and Discussion

The results presented in Figure 2 show that there is a large computational cost associated with determining upper and lower cutoff rigidities with errors $\leq$ 10%. The poor convergence of the lower cutoff rigidity in particular is noteworthy, e.g., R_L can change by as much as 10% when the rigidity space sampling density is increased from $10^5/R_C$ to $10^6/R_C$. The error associated with R_C with a similar sampling density is much less. R_C is determined to within 1% by sampling rigidity space with a density $\sim 1000/R_C$.

In a realistic quiet time geomagnetic field model (TS05Q), the relative error associated with scaling vertical cutoff rigidities from 100 km to 1000 km altitude is in general 1–4%, but maximum relative errors approach 10% in the midlatitudes and 20% near the polar cap boundaries. The $1/L_M^2$ scaling of vertical cutoffs improves at higher altitudes up to $\sim 6R_E$ in the quiet time field model, since the field becomes more dipole like at higher altitudes. If errors less than 10% are required, then a radial grid spacing of $\sim$ 100 km is needed near LEO, while

a grid spacing of ~1000 km is sufficient at 6 R_E. The situation is much worse during a severe geomagnetic storm, when the relative errors are 10–100% up to 2 R_E. In the TS05S field model, geomagnetic cutoffs drop to zero at and above ~4R_E.

The greatest relative errors associated with $1/L_M^2$ altitude scaling of the cutoff occur in the midlatitudes and near the polar cap boundaries. In the midlatitudes R_C is generally higher than R_M due to Earth's shadowing of trajectories near the cutoff. At low and high latitudes, R_C is generally lower and falls off more rapidly than R_M due to the presence of the open/closed field line boundary. In the IGRF model, the error is greatest in the midlatitudes, mainly due to the combined effect of the penumbra and an approximately 40°. Longitudinal phase shift between the maximum and minimum cutoff rigidity contours on the Earth's surface and the locations of maximum and minimum field strength, noted by *Smart and Shea* [1995]. In the TS05Q model fields, the error is greatest near the polar cap boundary where $1/L_M^2$ altitude scaling of the cutoff breaks down, since there is no open/closed field line boundary in a pure dipole field.

The NAIRAS atmospheric radiation model currently running at the NASA Langley Research Center uses a dynamic cutoff computation to model solar and galactic cosmic rays incident at the top of the Earth's atmosphere. Vertical cutoff rigidities are computed in TS05 model fields on a 5° × 5° latitude-longitude grid at 100 km using real-time solar wind and *Dst* data. The cutoff rigidities are updated once per hour, which is sufficient to capture typical storm time cutoff variations [e.g., see *Kress et al.*, 2010, Figure 6]. The cutoff computation requires 2.6 CPU hours (run on eight 2.5 GHz CPUs). At higher altitudes the range of latitudes over which the cutoff rigidity is nonzero is smaller, reducing computational time.

Results presented here show that a real-time data-driven cutoff computation extending over the inner magnetosphere is possible, using a medium sized cluster. Our planned future work includes development and implementation of a real-time data driven cutoff model of the Earth's inner magnetosphere.

Acknowledgments

This work was supported by the National Science Foundation awards ATM-0921979 and ATM-1023332. Support was also provided by NSF grant AGS-1023339. The Dartmouth College radiation belt and geomagnetic cutoff codes used to produce the results presented in this paper are freely available to the public and can be obtained by contacting the author at brian.kress@colorado.edu.

Yuming Wang thanks two anonymous reviewers for their assistance in evaluating this paper.

References

Cooke, D. J., J. E. Humble, M. A. Shea, D. F. Smart, N. Lurid, I. L. Rasmussen, B. Byrnak, P. Goret, and N. Petrou (1991), On cosmic-ray cut-off terminology, *Il Nuovo Cimento*, *14*, 213–234.

Fillius, R. W. (1968), Penetration of solar protons to four Earth radii in the equatorial plane, *Ann. Geophys.*, *24*, 821–840.

Kahler, S., and A. Ling (2002), Comparisons of high latitude E > 20 MeV proton geomagnetic cutoff observations with predictions of the SEPTR model, *Ann. Geophys.*, *20*(7), 997–1005.

Kress, B. T., C. J. Mertens, and M. Wiltberger (2010), Solar energetic particle cutoff variations during the 29–31 October 2003 geomagnetic storm, *Space Weather*, *8*, S05001, doi:10.1029/2009SW000488.

Kress, B. T., J. V. Rodriguez, J. E. Mazur, and M. Engel (2013), Modeling solar proton access to geostationary spacecraft with geomagnetic cutoffs, *J. Adv. Space Res.*, *52*, 1939–1948, doi:10.1016/j.asr.2013.08.019.

Lanzerotti, L. J. (1968), Penetration of solar protons and alphas to the geomagnetic equator, *Phys. Rev. Lett.*, *21*(13), 929–933.

Lemaitre, G., and M. S. Vallarta (1933), On Compton's latitude effect of cosmic radiation, *Phys. Rev.*, *43*(2), 87–91.

Leske, R. A., R. A. Mewaldt, and E. C. Stone (2001), Observations of geomagnetic cutoff variations during solar energetic particle events and implications for the radiation environment at the Space Station, *J. Geophys. Res.*, *106*(A12), 30,011–30,022.

McIlwain, C. E. (1961), Coordinates for mapping the distribution of trapped particles, *J. Geophys. Res*, *66*, 3681–3691.

Mertens, C. J., B. T. Kress, M. Wiltberger, S. R. Blattnig, T. S. Slaba, S. C. Solomon, and M. Engel (2010), Geomagnetic influence on aircraft radiation exposure during a solar energetic particle event in October 2003, *Space Weather*, *8*, S03006, doi:10.1029/2009SW000487.

Paulikas, G. A., and J. B. Blake (1969), Penetration of solar protons to synchronous altitude, *J. Geophys. Res.*, *74*(9), 2161–2168, doi:10.1029/JA074i009p02161.

Pchelkin, V. V., and E. V. Vashenyuk (2001), Effects of quasi-drift and problem cosmic ray penumbra, *Izv. RAN, Se. Fiz.*, *65*(3), 416–421.

Pchelkin, V. V., E. V. Pchelkina, and I. V. Golovchanskaya (2007), Anomalous behavior of cutoff rigidity variation in the region of the Mexico station during a magnetic superstorm on 20 November 2003, *Ann. Geophys.*, *25*, 1721–1725.

Ray, E. C. (1963), On the motion of charged particles in the geomagnetic field, *Ann. Phys.*, *24*, 1–18, doi:10.1016/0003-4916(63)90061-7.

Sauer, H. H. (1963), A new method of computing cosmic-ray cutoff rigidity for several geomagnetic field models, *J. Geophys. Res.*, *68*(4), 957–971, doi:10.1029/JZ068i004p00957.

Shea, M. A., D. F. Smart, and K. G. McCracken (1965), A study of vertical cutoff rigidities using sixth degree simulations of the geomagnetic field, *J. Geophys. Res.*, *70*, 4117–4130.

Shea, M. A., D. F. Smart, and L. C. Gentile (1985), The use of the McIlwain L-parameter to estimate cosmic ray vertical cutoff rigidities for different epochs of the geomagnetic field, *Proc. 19th Intl. Cosmic Ray Conf.*, *5*, 332–335.

Smart, D. F., and M. A. Shea (1994), Geomagnetic cutoffs: A review for space dosimetry applications, *Adv. Space Res.*, *14*(10), 787–797.

Smart, D. F., and M. A. Shea (1995), The difference between offset dipole coordinates and coordinates based on cutoff rigidity contours, in *24th International Cosmic Ray Conference*, vol. 4, edited by N. Iucci and E. Lamanna, pp. 1062–1065, Int. Union of Pure and Appl. Phys., Rome, Italy, 28 Aug.–8 Sep.

Smart, D. F., and M. A. Shea (2003), The space-developed dynamic vertical cutoff rigidity model and its applicability to aircraft radiation dose, *Adv. Space Res.*, *32*(1), 103–108, doi:10.1016/S0273-1177(03)90376-0.

Smart, D. F., and M. A. Shea (2009), Fifty years of progress in geomagnetic cutoff rigidity determinations, *Adv. Space Res.*, *44*, 1107–1123.

Smart, D. F., M. A. Shea, and R. Gall (1969), The daily variation of trajectory-derived high-latitude cutoff rigidities in a model magnetosphere, *J. Geophys. Res.*, *74*(19), 4731–4738, doi:10.1029/JA074i019p04731.

Smart, D. F., M. A. Shea, and E. O. Fluckiger (2000), Magnetospheric models and trajectory computations, *Space Sci. Rev.*, *93*(1–2), 305–333, doi:10.1023/A:1026556831199.

Smart, D. F., M. A. Shea, A. J. Tylka, and P. R. Boberg (2006), A geomagnetic cutoff rigidity interpolation tool: Accuracy verification and application to space weather, *Adv. Space Res.*, *37*(6), 1206–1217, doi:10.1016/j.asr.2006.02.011.

Störmer, C. (1955), *The Polar Aurora*, Oxford Univ. Press, London, England.

Swann, W. F. (1933), Application of Liouville's theorem to electron orbits in the Earth's magnetic field, *Phys. Rev.*, *44*(3), 224–227.

Taylor, H. E. (1967), Latitude local-time dependence of low-energy cosmic-ray cutoffs in a realistic geomagnetic field, *J. Geophys. Res.*, *72*(17), 4467–4470, doi:10.1029/JZ072i017p04467.

Tsyganenko, N. A., and M. I. Sitnov (2005), Modeling the dynamics of the inner magnetosphere during strong geomagnetic storms, *J. Geophys. Res.*, *110*, A03208, doi:10.1029/2004JA010798.

Tylka, A. J., C. M. S. Cohen, W. F. Dietrich, M. A. Lee, C. G. Maclennan, R. A. Mewaldt, C. K. Ng, and D. V. Reames (2005), Shock geometry, seed populations, and the origin of variable elemental composition at high energies in large gradual solar particle events, *Astrophys. J.*, *625*, 474–495.